NASA Technical Memorandum 101713

Preliminary Results From a Subsonic High Angle-of-Attack Flush Airdata Sensing (HI-FADS) System: Design, Calibration, and Flight Test Evaluation

Stephen A. Whitmore and Timothy R. Moes
Ames Research Center, Dryden Flight Research Facility, Edwards, California

Terry J. Larson
Analytical Mechanics Associates, Hampton, Virginia

1990

National Aeronautics and
Space Administration
Ames Research Center
Dryden Flight Research Facility
Edwards, California 93523-5000

PRELIMINARY RESULTS FROM A SUBSONIC HIGH ANGLE-OF-ATTACK FLUSH AIRDATA SENSING (HI-FADS) SYSTEM: DESIGN, CALIBRATION, ALGORITHM DEVELOPMENT, AND FLIGHT TEST EVALUATION

Stephen A. Whitmore* and Timothy R. Moes*
NASA Ames Research Center
Dryden Flight Research Facility
Edwards, California

and

Terry J. Larson**
Analytical Mechanics Associates
Hampton, Virginia

Abstract

A nonintrusive high angle-of-attack flush airdata sensing (HI-FADS) system was installed and flight-tested on the F-18 high alpha research flight vehicle at the National Aeronautics and Space Administration Ames Research Center's Dryden Flight Research Facility. The system is a matrix of 25 pressure orifices in concentric circles on the nose of the vehicle. The orifices determine angles of attack and sideslip, Mach number, and pressure altitude. Pressure was transmitted from the orifices to an electronically scanned pressure module by lines of pneumatic tubing. The HI-FADS system was calibrated and demonstrated using dutch roll flight maneuvers covering large Mach, angle-of-attack, and sideslip ranges. Reference airdata for system calibration were generated by a minimum variance estimation technique blending measurements from two wingtip airdata booms with inertial velocities, aircraft angular rates and attitudes, precision radar tracking, and meteorological analyses. The pressure orifice calibration was based on identifying empirical adjustments to modified Newtonian flow on a hemisphere. Calibration results are presented. Flight test results used all 25 orifices or used a subset of 9 orifices. Under moderate maneuvering conditions, the HI-FADS system gave excellent results over the entire subsonic Mach number range up to 55° angle of attack. The internal pneumatic frequency response of the system is accurate to beyond 10 Hz. Aerodynamic lags in the aircraft flow field caused some performance degradation during heavy maneuvering.

Nomenclature

A	aerodynamic model coefficient
B	aerodynamic model coefficient
C	linearized observation matrix
C_p	pressure coefficient
ESP	electronically scanned pressure
$F[\ldots]$	aerodynamic model functional
HARV	high alpha research vehicle
HI-FADS	high angle-of-attack flush airdata sensing
INS	inertial navigation system
i	HI-FADS port index
j	iteration index
M_∞	free-stream Mach number
N	number of HI-FADS pressure observations used
PCM	pulse code modulation
PSD	power spectral density
p	HI-FADS surface pressure
p_∞	free-stream static pressure
q_{c_∞}	free-stream compressible dynamic pressure
$\bar{q}_\infty$	free-stream incompressible dynamic pressure
R	surface position vector
rms	root mean square
V	velocity vector
X	HI-FADS state vector
Z	HI-FADS pressure observation vector
α	angle of attack, deg
α_e	effective angle of attack, deg
α_∞	free-stream angle of attack, deg
β	angle of sideslip, deg
β_e	effective angle of sideslip, deg
β_∞	free-stream angle of sideslip, deg

*Aerospace Engineer. Member AIAA.
**Engineer. Member AIAA.

$\Delta\alpha$	angle-of-attack residual, deg
$\delta\alpha$	angle-of-attack calibration parameter, $(\alpha_e - \alpha_\infty)$, deg
$\Delta\beta$	angle-of-sideslip residual, deg
$\delta\beta$	angle-of-sideslip calibration parameter, $(\beta_e - \beta_\infty)$, deg
ΔM	Mach number residual
δX	state vector iteration error
δZ	model prediction iteration error
ϵ	HI-FADS model calibration factor
ϵ_M	variation of ϵ with Mach number
ϵ_α	variation of ϵ with effective angle of attack
θ	flow incidence angle, deg
λ	HI-FADS normal angle coordinate, deg
σ	standard deviation of HI-FADS pressure vector
ϕ	HI-FADS clock angle coordinate, deg

Introduction

Current aircraft performance and maneuverability requirements have complicated the problem of flight control augmentation. This is especially true at high angles of attack where small changes in angle of attack can greatly influence the aerodynamic properties of the aircraft. To study aerodynamics at high angles of attack, a flight test program with the F-18 high alpha research vehicle (HARV) is being conducted at the National Aeronautics and Space Administration Ames Research Center's Dryden Flight Research Facility. Preliminary flights have concluded. To achieve the program's research objectives, highly accurate airdata measurements were required throughout the entire subsonic flight envelope. At high angles of attack, it is difficult to measure airdata accurately with traditional sensing devices such as nosebooms. Also, a noseboom installation alters the basic flow characteristics of the aircraft nose. Since flow visualization and aircraft parameter identification at high angles of attack were major HARV program objectives, it was critical not to alter this flow.[1]

To avoid this difficulty, a nonintrusive high angle-of-attack flush airdata sensing (HI-FADS) system was installed and flight-tested on the HARV. The HI-FADS system design is an evolution of prototype nonintrusive systems demonstrated in previous flight research studies.[2,3,4] References 3 and 4 give individual orifice pressure coefficient data for similar arrays on other aircraft. This paper emphasizes the airdata algorithm development and composite results expressed as airdata parameter estimates and describes the HI-FADS system hardware, calibration techniques, and algorithm development. An independent empirical verification was performed over a large portion of the subsonic flight envelope. Test points were obtained for Mach numbers from 0.15 to 0.94, and angles of attack from −8.0 to 55.0°. Angles of sideslip ranged from −15.0 to 15.0°, and test altitudes ranged from 18,000 to 40,000 ft.

Vehicle Description

The HARV (Fig. 1) is a single-place F-18 aircraft with dual engines and a midwing with leading- and trailing-edge flaps. The noseboom was removed to allow the HI-FADS to be installed. The wingtip sidewinder launch racks were removed and replaced with camera pods and wingtip airdata booms. For flight safety, the HARV flight tests were limited to 55° angle of attack.

Research Measurement Aquisition System

For the HARV flight tests a special research measurement aquisition system was installed. This system provided flight research measurements in addition to the data provided by the aircraft flight systems sensors. Research system measurements included: (1) linear accelerations from a set of body-axis accelerometers, (2) pitch, roll, and yaw attitudes from a gimbaled attitude gyro, (3) three-axis angular velocities from a body-axis rate-gyro package, (4) airdata from two calibrated wingtip airdata booms, and (5) pressure data from the HI-FADS system. Velocity, aircraft attitudes, and altitude from the aircraft inertial navigation system (INS) were also interfaced with the research measurement aquisition system. All data were digitally encoded onboard using pulse code modulation (PCM) and telemetered to the ground where they were displayed in real time and recorded for post-flight analysis.

The wingtip airdata booms were installed specifically for the HARV flight tests. The right wingtip airdata boom was a standard National Advisory Committee for Aeronautics (NACA) pitot-static head with flow direction vanes.[5] The left wingtip airdata boom was a specially constructed swivel-head designed to align with the local air-velocity vector. This swivel design eliminated total pressure loss at high angles of attack. Flow direction sensing vanes were also installed on the left wingtip boom. Both wingtip booms were calibrated to a steady-state bias accuracy of better than ±0.003 in Mach number and ±0.5° in angle of attack and sideslip. The validity range for the calibration of the wingtip airdata sensors was up to 40° angle of attack. Beyond this the accuracy of the wingtip sensor measurements diminished rapidly.

The HI-FADS configuration has a simple hardware arrangement. The basic fixture is a small fiberglass-reinforced plastic cap, mounted on the nose of the F-18 HARV aircraft. A set of 25 0.06-in.-diameter pressure orifices, arranged in annular rings, were drilled in the nosecap. Flight tests were conducted using both a 25-port arrangement and a subset of 9 ports. Pressures at the nosecap were sensed by a multitransducer electronically scanned pressure (ESP) module remotely mounted on a structural bulkhead within the

aircraft nose cavity. Each ESP transducer has an internal volume of less than 0.01 in^3. The temperature enviorment of the ESP module was controlled by wrapping the sensor in a heater blanket to maintain the entire unit at an operating temperature of approximately 110 °F. The rear reference pressure for the ESP module (which consists of differential pressure sensors) was measured by an absolute pressure sensor also mounted in the aircraft nose cavity. Short-period fluctuations in the reference pressure were damped out by a reference tank with an internal volume of approximately 5 in^3. The temperature environment of the reference pressure sensor was also controlled by a heater blanket.

The outputs from both the ESP module and the reference sensor were discretized by PCM and telemetered to the ground using the research measurement aquisition system. Data were sampled at 50 samples/sec. Depending on the scaled pressure ranges, which varied from ±4.0 to ±5.0 lb/in^2, the resolution of each recorded ESP pressure signal varied from 1.0 to 2.0 lb/ft^2 for each PCM count. The estimated accuracy was approximately ±0.25 percent of full-scale. The resolution of the reference static pressure sensor was 0.015 lb/ft^2 for each PCM count. Again, the estimated accuracy was on the order of ±0.05 percent of full-scale. The HI-FADS hardware arrangement is shown in Fig. 2.

Potential resonance and aliasing problems with the HI-FADS pressure measurements were circumvented by careful selection of the pneumatic lines used to transmit pressure impulses from the HI-FADS surface ports to the ESP module. Through previous dynamic response data for similar installations and the analysis techniques presented in Ref. 6, it was determined that at a representative altitude of 20,000 ft, 8 ft of 0.06-in.-diameter flexible tubing connecting the HI-FADS ports to the ESP module would approximate a low pass filter with a rolloff frequency of 20 to 30 Hz. In the 20–30 Hz frequency range the pneumatic power is attenuated by approximately 3 dB and the pneumatic lag is approximately 10 msec. These attenuations and lags are considered acceptable. For a lower altitude the attenuation and lag will be less; for a higher altitude they will be greater. Figure 3 shows the frequency response of the pneumatic tubing and ESP port configuration at 20,000-ft altitude.

The HI-FADS pressure port layout consists of a set of 25 ports arranged in four rings and a single nosetip port. The rings were distributed in a symmetric radial pattern around the nosecap axis of symmetry. Analyses were performed using all 25 orifices and a subset of 9 orifices. The locations of the nosecap ports were determined using a normal/clock angle (Fig. 4) coordinate system measured relative to the axis of symmetry. The nosecap itself is biased downward at an angle of 5.6° relative to the longitudinal axis of the aircraft. The normal angle (λ) is defined as the total angle that the normal to the surface makes with respect to the nosecap axis of symmetry. The clock angle (ϕ) is defined as the angle, looking aft, around the axis of symmetry, measured clockwise, starting at the aircraft Z-axis.

The ports were named according to the clockwise order of occurence within each annular ring, starting at $\phi = 0$. Thus, the third clockwise port in the second ring is designated P203, the fourth port in the second ring is designated P204, and so on. The coordinate angles of the various pressure ports are listed in Table 1. Port numbers followed by an asterisk were used in both the 9-port and 25-port analyses.

Flow Analysis and Pressure Modeling

In this section, a flow model is developed which can relate the HI-FADS pressure measurements to free-stream airdata quantities. Once a model is developed and verified, all 25 pressure measurements can be used along with the model to estimate the complete airdata state using nonlinear regression. The use of an overdetermined (more observations than states) analysis minimizes the effects of error of any single pressure measurement. This results in a robust algorithm. First a potential flow pressure coefficient model will be developed; then effects caused by aircraft induced upwash and sidewash will be modeled.

Pressure Coefficient Model for Incompressible Potential Flow on a Hemisphere

References 7 and 8 show that for three-dimensional incompressible potential flow around a sphere, the pressure coefficient at the surface is

$$C_p(\theta) = 1 - \frac{9}{4}\sin^2(\theta) = -\frac{5}{4} + \frac{9}{4}\cos^2(\theta) \qquad (1)$$

where θ is the total flow incidence angle at the surface. To account for a nonspherical nose shape, compressibility, and afterbody effects, the coefficients assume arbitrary values while still retaining the basic form of the model

$$C_p(\theta) = A + B\ \cos^2(\theta) \qquad (2)$$

The coefficients A and B are empirically determined. To satisfy conservation of momentum and energy, the stagnation pressure constraint must be enforced, so that when $\theta = 0$

$$C_p(0) = \frac{q_c}{\bar{q}} = A + B \qquad (3)$$

This constraint may be built into the model by letting

$$A = \frac{q_c}{\bar{q}}\epsilon \qquad (4)$$

and

$$B = \frac{q_c}{\bar{q}}(1 - \epsilon) \qquad (5)$$

Substituting these constraints for A and B into equation (1) and regrouping terms gives

$$C_p(\theta) = \frac{q_c}{\bar{q}}[\cos^2(\theta) + \epsilon\ \sin^2(\theta)] \qquad (6)$$

Thus the parameter ϵ represents an adjustment to modified Newtonian flow theory.[2] Applying the definition of the pressure coefficient

$$C_p(\theta) = \frac{p_\theta - p_\infty}{\bar{q}} \tag{7}$$

the model reduces to

$$p_\theta = q_c[\cos^2(\theta) + \epsilon \sin^2(\theta)] + p_\infty \tag{8}$$

The incidence angle may be written in terms of angle of attack and angle of sideslip by taking the inner product of the position vector with the velocity vector

$$\cos(\theta) = \frac{V \times R}{\|V\| \|R\|} = \begin{aligned} &\cos(\alpha)\cos(\beta)\cos(\lambda) \\ &+ \sin(\beta)\sin(\phi)\sin(\lambda) \\ &+ \sin(\alpha)\cos(\beta)\cos(\phi)\sin(\lambda) \end{aligned} \tag{9}$$

Thus for a given location on the surface

$$p(\phi, \lambda) = F(\alpha, \beta, q_c, p_\infty, \phi, \lambda, \epsilon) \tag{10}$$

where α, β, q_c, and p_∞ are airdata parameters, ϕ and λ are orifice coordinate angles, and ϵ is a calibration parameter to be empirically determined.

Effects of Aircraft Induced Upwash and Sidewash

The potential flow model assumes a nonlifting hemisphere with no trailing afterbody. Clearly this is not true for the HARV HI-FADS where induced wash caused by aircraft lift and thickness alters the angle of attack and sideslip of the local stagnation streamline.[10] As a result, the HI-FADS system experiences effective (α_e, β_e) not free-stream (α_∞, β_∞) angles of attack and sideslip. To adjust the flow model for this difference let

$$\alpha_e = \alpha_\infty + \delta\alpha \tag{11}$$

and

$$\beta_e = \beta_\infty + \delta\beta \tag{12}$$

where $\delta\alpha$ and $\delta\beta$ are calibration factors which must be empirically identified.

System Calibration

The HI-FADS system was calibrated using reference airdata values generated from flight data by minimum variance estimation techniques.[9,10,11] In this procedure, high-accuracy, high-fidelity reference airdata are generated by merging complementary information from multiple data sources provided by the research data aquisition system with external measurements such as radar tracking and analyses of weather balloon information.

All flight maneuvers used in the calibration analyses were preceeded and followed by approximately 20 sec of stabilized low to moderate angle-of-attack flight. During this stabilized flight, the wingtip boom airdata were weighted heavily to give initial and final estimates of the atmospheric winds. During the course of the calibration maneuvers, filter weights were adaptively varied to weight the wingboom airdata inversely proportional to both pitch rate and angle of attack. At the same time, the equivalent time constant of the wind states was increased in direct proportion to pitch rate and angle of attack. Weights on the inertial and meteorological data were constant throughout the maneuver. Maneuver reference airdata were generated off-line using a forward–filter, backward–smoother algorithm and stored for later use in the calibration analyses.

A maneuver was good for calibration purposes when the resulting wind estimates showed little or no correlation to aircraft dependent velocity parameters. The basic premise of this technique is that if atmospheric winds change during the course of a flight maneuver, they should change independent of aircraft motions. Examining filter covariance estimates shows that the resulting reference airdata estimates have a root mean square (rms) noise level of approximately 0.001 in Mach number, 0.1° in angle of attack and angle of sideslip, and 10 ft in altitude.

Estimation of Calibration Parameters Using Reference Airdata

The calibration parameters $\delta\alpha$, $\delta\beta$, and ϵ were estimated by substituting the reference airdata into the flow model and comparing the model-predicted pressures to the measured pressures. Residuals between the measured and predicted pressures were used to infer the values of the calibration parameters at each data frame using nonlinear regression.

The pressure at the ith HI-FADS orifice is related to the flow indicence angle according to the semi-empirical expression

$$p_i = q_c[\cos^2(\theta_i) + \epsilon \sin^2(\theta_i)] + p_\infty \tag{13}$$

where θ_i is a function of the surface location and the effective angles of attack and sideslip. Equation (13) may be written as

$$p_i = F\left\{ \begin{pmatrix} \alpha_e \\ \beta_e \\ p_\infty \\ q_c \\ \epsilon \end{pmatrix}, \begin{pmatrix} \phi_i \\ \lambda_i \end{pmatrix} \right\} \tag{14}$$

where

$$\begin{pmatrix} \phi_i \\ \lambda_i \end{pmatrix}$$

is the coordinate vector for the ith HI-FADS orifice. If equation (14) is linearized by expanding in a power series around

$$\begin{pmatrix} \alpha_e \\ \beta_e \\ \epsilon \end{pmatrix} = \begin{pmatrix} \alpha_\infty \\ \beta_\infty \\ 0 \end{pmatrix} \tag{15}$$

truncated after first order, and evaluated using the measured pressures and reference airdata, the result may be grouped

as the linear matrix system,

$$\begin{pmatrix} p_1 - F_{1_{|\infty}} \\ p_2 - F_{2_{|\infty}} \\ \vdots \\ p_N - F_{N_{|\infty}} \end{pmatrix} = \begin{pmatrix} \left(\frac{\partial F_1}{\partial \alpha}\right)_{|\infty} & \left(\frac{\partial F_1}{\partial \beta}\right)_{|\infty} & \left(\frac{\partial F_1}{\partial \epsilon}\right)_{|\infty} \\ \left(\frac{\partial F_2}{\partial \alpha}\right)_{|\infty} & \left(\frac{\partial F_2}{\partial \beta}\right)_{|\infty} & \left(\frac{\partial F_2}{\partial \epsilon}\right)_{|\infty} \\ \vdots & \vdots & \vdots \\ \left(\frac{\partial F_N}{\partial \alpha}\right)_{|\infty} & \left(\frac{\partial F_N}{\partial \beta}\right)_{|\infty} & \left(\frac{\partial F_N}{\partial \epsilon}\right)_{|\infty} \end{pmatrix} \times \begin{pmatrix} \delta\alpha \\ \delta\beta \\ \epsilon \end{pmatrix} \quad (16)$$

where

$$F_{i_{|\infty}} = F\left\{ \begin{pmatrix} \alpha_\infty \\ \beta_\infty \\ p_\infty \\ q_{c_\infty} \\ 0 \end{pmatrix}, \begin{pmatrix} \phi_i \\ \lambda_i \end{pmatrix} \right\} \quad (17)$$

and

$$\left(\frac{\partial F_i}{\partial \alpha}\right)_{|\infty} = \frac{\partial F}{\partial \alpha}\left\{ \begin{pmatrix} \alpha_\infty \\ \beta_\infty \\ p_\infty \\ q_{c_\infty} \\ 0 \end{pmatrix}, \begin{pmatrix} \phi_i \\ \lambda_i \end{pmatrix} \right\} \quad (18)$$

and so on. At each data frame equation (16) is solved for the calibration parameters $\delta\alpha$, $\delta\beta$, and ϵ using least-squares regression.[12]

Calibration Results

During the course of the calibration procedure, data were obtained throughout the subsonic flight regime. Mach numbers ranged from 0.15 to 0.94, angles of attack from -8.0 to 55.0°, and angles of sideslip from -15.0 to 15.0°. Various maneuvers such as pushover-pullups, level acceleration-decelerations, angle-of-sideslip sweeps, and wingrocks were examined. Calibrations were performed for both the 9-port and 25-port configurations.

Systematic trends were identified by plotting the estimated calibration parameters, the results of the regression on equation (16), as a function of various flight variables and visually inspecting the results. Once trends were identified by visual inspection, they were curve-fit and interpolated to generate a series of tabular breakpoints which were hard-coded into the HI-FADS algorithm. Because the HI-FADS system measures effective not free-stream angles of attack and sideslip, calibration results will be presented in terms of the effective flow angles. Calibration results did not differ significantly for the 9-port and 25-port configurations.

Calibration data for the upwash parameter $\delta\alpha$ are shown in Fig. 5. The upwash parameter is plotted on the ordinate axis, and the effective angle of attack, as measured by the HI-FADS system, is plotted on the abscissa. While the standard deviation in the upwash parameter increases with decreasing Mach number, no trend of upwash parameter with either Mach number or angle of sideslip was clearly discernable.

Similar calibration data for the sidewash parameter $\delta\beta$ are shown in Fig. 6. The sidewash parameter is plotted on the ordinate axis; the effective angle of sideslip, as measured by the HI-FADS system, is plotted on the abscissa. As above, the standard deviation in sidewash parameter increased with decreasing Mach number, while the sidewash parameter had no systematic trend with either Mach number or angle of attack.

During the course of the analysis, it was empirically determined that the calibration factor ϵ may be decomposed into two components: one which varies as a function of Mach number only (ϵ_M), and one which varies as a function of effective angle of attack only (ϵ_α), where

$$\epsilon = \epsilon_M + \epsilon_\alpha$$

These breakpoints are shown in Figs. 7 and 8. In Fig. 7, ϵ_M is plotted on the ordinate axis, while free-stream Mach number is plotted on the abscissa. Interestingly, the break points of Fig. 7 agree closely with the curve prescribed by the Prantl-Glauret transformation, where

$$\frac{1}{\sqrt{1 - M_\infty^2}}$$

is plotted as a function of free-stream Mach number. This curve is shown as a solid line on these plots. Prantl-Glauret is the affine transformation used subsonically to map incompressible flows into equivalent compressible flows.[9,10] Thus, ϵ_M may be thought of as a compressibility correction on the potential model.

In Fig. 8, ϵ_α is plotted on the ordinate axis, while effective angle of attack is plotted on the abscissa. Stagnation pressure data presented in Ref. 13 indicate that ϵ_α may be considered as an adjustment for the loss of total flow energy at the HI-FADS sensing array caused by the increasing average flow angularity over all the pressure ports. For the moderate angles of sideslip encountered in the HARV HI-FADS tests, no systematic trend relating angle of sideslip to ϵ was found.

Developing the Algorithm

The algorithm used for determining the free-stream airdata parameters (α_∞, β_∞, p_∞, and q_{c_∞}) with the HI-FADS pressure data was developed by an approach similar to that of the previous section. Assuming that an estimate of the jth free-stream airdata state is available, if the calibrated flow

model is expanded and linearized about this estimate

$$\begin{pmatrix} p_{1_{j+1}} - F_{1_{|_j}} \\ p_{2_{j+1}} - F_{2_{|_j}} \\ \vdots \\ p_{N_{j+1}} - F_{N_{|_j}} \end{pmatrix} =$$

$$\begin{pmatrix} \left(\frac{\partial F_1}{\partial \alpha}\right)_{|_j} & \left(\frac{\partial F_1}{\partial \beta}\right)_{|_j} & \left(\frac{\partial F_1}{\partial p_\infty}\right)_{|_j} & \left(\frac{\partial F_1}{\partial q_{c_\infty}}\right)_{|_j} \\ \left(\frac{\partial F_2}{\partial \alpha}\right)_{|_j} & \left(\frac{\partial F_2}{\partial \beta}\right)_{|_j} & \left(\frac{\partial F_2}{\partial p_\infty}\right)_{|_j} & \left(\frac{\partial F_2}{\partial q_{c_\infty}}\right)_{|_j} \\ \vdots & \vdots & \vdots & \vdots \\ \left(\frac{\partial F_N}{\partial \alpha}\right)_{|_j} & \left(\frac{\partial F_N}{\partial \beta}\right)_{|_j} & \left(\frac{\partial F_N}{\partial p_\infty}\right)_{|_j} & \left(\frac{\partial F_N}{\partial q_{c_\infty}}\right)_{|_j} \end{pmatrix} \quad (19)$$

$$\times \begin{pmatrix} \alpha_{\infty_{j+1}} - \alpha_{\infty_j} \\ \beta_{\infty_{j+1}} - \beta_{\infty_j} \\ p_{\infty_{j+1}} - p_{\infty_j} \\ q_{c_{\infty_{j+1}}} - q_{c_{\infty_j}} \end{pmatrix}$$

where

$$F_{i_{|_j}} = F\left\{ \begin{pmatrix} \alpha_{\infty_j} \\ \beta_{\infty_j} \\ p_{\infty_j} \\ q_{c_{\infty_j}} \end{pmatrix}, \begin{pmatrix} \delta\alpha \\ \delta\beta \\ \epsilon \end{pmatrix}, \begin{pmatrix} \phi_i \\ \lambda_i \end{pmatrix} \right\} \quad (20)$$

and so on. The parameters $\delta\alpha$, $\delta\beta$, and ϵ are computed using the calibration tables. If the left side of equation (19) is evaluated using measured pressure data, the N by 4 dimensional overdetermined linear system may be written in matrix form as

$$\delta Z = C\ \delta X\ +\ \text{error} \quad (21)$$

and solved using weighted iterative least squares[12]

$$\hat{X}_{j+1} = \hat{X}_j + [\ (C^T C)^{-1} C^T\ ][Z_{j+1} - \hat{Z}_j] \quad (22)$$

with

$$Z_{j+1} = \begin{pmatrix} p_{1_{j+1}} \\ p_{2_{j+1}} \\ \vdots \\ p_{N_{j+1}} \end{pmatrix}, \quad \hat{Z}_j = \begin{pmatrix} \hat{F}_{1_{|_j}} \\ \hat{F}_{2_{|_j}} \\ \vdots \\ \hat{F}_{N_{|_j}} \end{pmatrix} \quad (23)$$

and

$$\hat{X}_{j+1} = \begin{pmatrix} \hat{\alpha}_{\infty_{j+1}} \\ \hat{\beta}_{\infty_{j+1}} \\ \hat{p}_{\infty_{j+1}} \\ \hat{q}_{c_{\infty_{j+1}}} \end{pmatrix}, \quad \hat{X}_j = \begin{pmatrix} \hat{\alpha}_{\infty_j} \\ \hat{\beta}_{\infty_j} \\ \hat{p}_{\infty_j} \\ \hat{q}_{c_{\infty_j}} \end{pmatrix} \quad (24)$$

and so on.

At each data frame the algorithm must be iterated until convergence; this typically takes two iterations. To aid convergence at the end of each data frame, the system is relinearized around the state estimate resulting from the previous data frame. Initially, the system is linearized using INS data until startup transients have disappeared. This initialization has also been performed with a prescribed set of initial conditions.

Sensor fault detection is mechanized using a simple 3σ error bound. At the beginning of each data frame, the mean and standard deviation of the sensor pressure array are evaluated. The weight of any sensor whose reading deviates from the mean by more than 3 times the standard deviation 3σ is set to 0.001. All sensors with readings not exceeding the 3σ bound are given a weight of 1.0. This relative weighting scheme, verified using simulated data, effectively eliminates incoming information from a deviant sensor. This weighting scheme is not intended to enhance the HI-FADS algorithm estimates, but only to detect catastrophic failure of any sensor. The algorithm robustness accounts for small deviations in sensor readings.

Evaluation of System Performance

The performance of the HI-FADS system was evaluated using flight data. Various HI-FADS derived airdata estimates were compared to the corresponding reference airdata parameters. The reference airdata were generated using the same minimum variance estimation techniques described previously. To show typical flight results, data from a single, moderate rate dutch roll maneuver will be presented. These results, performed with the 9-port configuration, were not used in establishing the calibration tables.

Comparisons of HI-FADS with reference angles of attack are shown in Fig. 9. Figure 9(a) shows the actual angle-of-attack time histories. Two curves are presented, the reference angle of attack and the HI-FADS angle of attack. For the scale used, no differences are discernable. Actual differences may be seen by plotting the time history of the residual between the HI-FADS and reference angles of attack. This residual time history is presented in Fig. 9(b). Similar comparisons for Mach number and angle of sideslip are presented in Figs. 10(a), 10(b), 11(a), and 11(b). Except for small deviations during the high-rate portions of the maneuver, it is difficult to find any difference between the HI-FADS and reference airdata values.

Quantitative accuracy levels were obtained by evaluating residual statistics for a variety of HI-FADS maneuvers. Table 2 presents results for both the 9-port the 25-port analyses. Eight flight maneuvers, obtained during several different flights, were used to perform the statistical evaluation for the 9-port analyses. Six of the above maneuvers were used to perform the statistical evaluation for the 25-port analyses. During several data flights at high angles of attack some of the ports were used for flow visualization studies and were disconnected from the ESP module. Thus the full 25-port analyses could not be performed for these flights. Approximately 45,000 data frames were used to perform the 9-port statistical evaluation. Approximately 26,000 data frames were used to perform the 25-port statistical analysis.

HI-FADS airdata estimates from 25-port analyses were slightly less noisy than for the 9-port analyses. Since the 25-port configuration is more overdetermined and thus less sensitive to individual measurement errors, this result is expected. The statistical data indicate that even up to high

angles of attack both the 9-port and 25-port configurations have a standard deviation of approximately 0.5° in angle of attack and angle of sideslip, and better than 0.004 in Mach number. On a steady-state basis the extremely low residual mean values indicate that the HI-FADS system can be calibrated as accurately as the reference against which it is compared.

Some discussion concerning the effects of unsteady aerodynamics on the HI-FADS frequency response is appropriate. Recall that the flow field at the aircraft nose is influenced by the circulation field originating at the aircraft center of pressure. The strength of this circulation field is directly proportional to the aircraft lift and thus indirectly correlated to the aircraft angle of attack. As the aircraft angle of attack varies, it takes a finite amount of time for changes in the circulation field to develop and propogate forward from the center of pressure. This propogation delay results in a phase lag in the HI-FADS airdata measurements. At 20,000 ft altitude and Mach 0.6, data analyses have shown this delay to be approximately 100 msec.

Power spectral density (PSD) analysis indicates that the HI-FADS measurements are valid through 10 Hz. This conclusion is shown in Figs. 12 and 13. In these figures the PSD of HI-FADS angle of attack and Mach number from the dutch roll maneuver of Figs. 9 and 10 are plotted. In both figures the magnitude rolloff occurs around 10 Hz and reaches the noise threshold of the measurement system a little beyond 20 Hz. Because the atmospheric spectrum for this particular maneuver has not been independently identified using other data sources, it is unclear whether the rolloff from 10 to 20 Hz is a result of HI-FADS system pressure attenuation or caused by a decrease in power of the free-stream turbulence at these frequencies. In any case the HI-FADS dynamic response to beyond 10 Hz exceeds the dynamic response capability of most production airdata systems.

Under moderate maneuvering conditions, (angular rates less than 20 deg/sec) all flight data examined show that the HI-FADS system, in both the 9-port and 25-port configurations, performs well over the entire subsonic Mach number range and up to 55° angle of attack. During heavy maneuvering (angular rates greater than 20 deg/sec), aerodynamic lags in the aircraft flow field cause some performance degradation. The frequency response of the system is good through 10 Hz.

The preliminary flight results demonstrate that the calibration of the HI-FADS system needs further refinement to achieve greater system accuracy and expand the validity range to higher angles of attack and to supersonic flight. The frequency response capability must be studied further to determine the operational limits of the HI-FADS system. Techniques for interfacing the HI-FADS data with INS data should be addressed to improve accuracy over a larger flight envelope. Onboard avionics and processors required for a real-time HI-FADS implementation should be developed, installed, and tested on a flight vehicle.

Concluding Remarks

A protype nonintrusive airdata system was installed and flight-tested subsonically at high angles of attack on the F-18 high alpha research flight vehicle at NASA Ames Research Center's Dryden Flight Research Facility. This system consists of a matrix of 25 pressure orifices arranged in concentric circles on the nose of the vehicle. The system was tested using all 25 pressure ports and a subset of 9 pressure ports. Pressure was transmitted from the orifices to a multiport electronically scanned pressure module through lines of flexible pneumatic tubing. Outputs were digitized and telemetered to the ground where they were recorded on tape for post-flight processing.

The high angle-of-attack flush airdata sensing (HI-FADS) system was calibrated using flight data. The calibration parameters relate effective angle of attack and angle of sideslip to free-stream values and account for compressibility and total energy loss at the sensor array. Details of the calibration procedure and calibration results were presented.

The HI-FADS algorithm was developed and presented. Flight results were processed and compared against reference airdata. Statistical analysis of residuals for both the 9-port and the 25-port configurations indicate that the random measurement uncertainty is approximately 0.5° in angle of attack and angle of sideslip, and less than 0.004 in Mach number. The extremely low residual mean values indicate that on a steady-state basis the HI-FADS system can be calibrated as accurately as the reference values to which the system is calibrated.

Spectral response characteristics of the HI-FADS system were examined. The power spectral density data show that the frequency response of the system is good beyond 10 Hz. Under moderate maneuvering conditions (angular rates less than 20 deg/sec), the HI-FADS system gave excellent results over the entire subsonic Mach number range and up to 55° angle of attack. During heavy maneuvering (angular rates greater than 20 deg/sec), aerodynamic lags in the aircraft flow field cause some performance degradation.

The calibration of the HI-FADS system needs further development to expand the validity range to higher angles of attack and to transonic and supersonic flight regimes. Local aerodynamic effects on the frequency response must be studied further. At the higher subsonic Mach numbers the frequency response problem may need to be solved by the development of an inertial–HI-FADS hybrid system. Onboard avionics and processors required for a real-time HI-FADS implementation should be developed, installed, and tested on a flight vehicle.

References

[1]Fisher, David F., Del Frate, John H., and Richwine, David M., "In-Flight Flow Visualization Characteristics of the NASA F-18 High Alpha Research Vehicle Aircraft at High Angles of Attack," SAE Paper 89-2222, Sept. 1989.

[2] Henry, M.W., Wolf, H., and Siemers, Paul M., III, "Shuttle Entry Airdata System (SEADS): Optimization of Preflight Algorithm Based on Flight Results," 15th Aerodynamic Testing Conference, AIAA 88-2053, May 1988.

[3] Larson, Terry J., Whitmore, Stephen A., Ehernberger, L.J., Johnson, J. Blair, and Siemers, Paul M., III, *Qualitative Evaluation of a Flush Air Data System at Transonic Speeds and High Angles of Attack*, NASA TP-2716, 1987.

[4] Larson, Terry J., and Siemers, Paul M., III, *Subsonic Investigation of an All Flush Orifices Airdata System*, NASA TP-1643, 1980.

[5] Richardson, Norman R., and Pearson, Albin O., *Wind-Tunnel Calibrations of a Combined Pitot-Static Tube, Vane-Type Flow-Direction Transmitter, and Stagnation-Temperature Element at Mach Numbers from 0.60 to 2.87*, NASA TN D-122, 1959.

[6] Whitmore, Stephen A., *Formulation of a General Technique for Predicting Pneumatic Attenuation Errors in Airborne Pressure Sensing Devices*, NASA TM-100430, 1988.

[7] Currie, I.G., *Fundamental Mechanics of Fluids*, McGraw-Hill Book Company, New York, 1974.

[8] Kuethe, Arnold M., and Chow, Cheun-Yen, *Foundations of Aerodynamics: Bases of Aerodynamic Design*, Third Edition, John Wiley and Sons, New York, 1976.

[9] Whitmore, Stephen A., "Reconstruction of the Shuttle Reentry Air Data Parameters Using a Linearized Kalman Filter," Atmospheric Flight Mechanics Conference, AIAA 83-2097, Aug. 1983.

[10] Whitmore, Stephen A., *Formulation and Implementation of A Non-Stationary Adaptive Estimation Algolirithm with Applications to Air-Data Reconstruction*, NASA TM-86727, 1985.

[11] Whitmore, Stephen A., Larson, Terry J., and Ehernberger, L.J., *Air Data Position-Error Calibration Using State Reconstruction Techniques*, NASA TM-86029, 1984.

[12] Brogran, William L., *Modern Control Theory*, Quantum Publishers, Inc., New York, 1974.

[13] Gracey, William, *Measurement of Aircraft Speed and Altitude*, NASA RP-1046, 1980.

Table 1. The HARV HI-FADS pressure port locations.

Port	Clock angle, deg	Normal angle, deg
P001*	0.0	0.0
P101	0.0	20.0
P102	90.0	20.0
P103	180.0	20.0
P104	270.0	20.0
P201	0.0	40.0
P202	90.0	40.0
P203	180.0	40.0
P204	270.0	40.0
P301*	0.0	55.0
P302	45.0	55.0
P303*	90.0	55.0
P304	135.0	55.0
P305*	180.0	55.0
P306	225.0	55.0
P307*	270.0	55.0
P308	315.0	55.0
P401	0.0	60.0
P402*	45.0	60.0
P403	90.0	60.0
P404*	135.0	60.0
P405	180.0	60.0
P406*	225.0	60.0
P407	270.0	60.0
P408*	315.0	60.0

*Used for nine-port analyses.

Table 2. The HARV HI-FADS airdata residual statistics for 9-port and 25-port configurations.

	9-port		25-port	
Parameter	Mean error	rms error	Mean error	rms error
Angle of attack, deg	0.02	0.56	0.02	0.48
Angle of sideslip, deg	0.10	0.52	0.10	0.46
Mach number	0.0008	0.004	0.0007	0.003
Altitude, ft	11.4	19.2	9.2	16.3
Airspeed, ft/sec	0.84	4.00	0.75	3.00

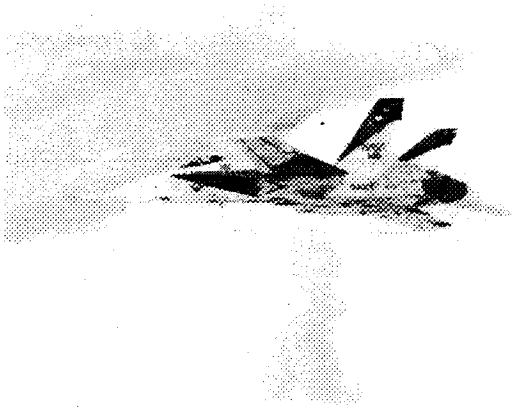

Fig. 1 The high alpha research vehicle.

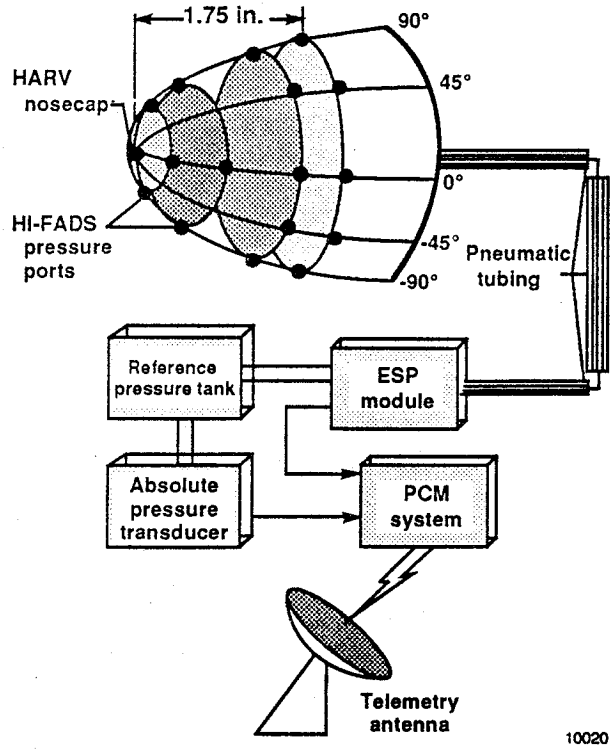

Fig. 2 The HI-FADS system hardware.

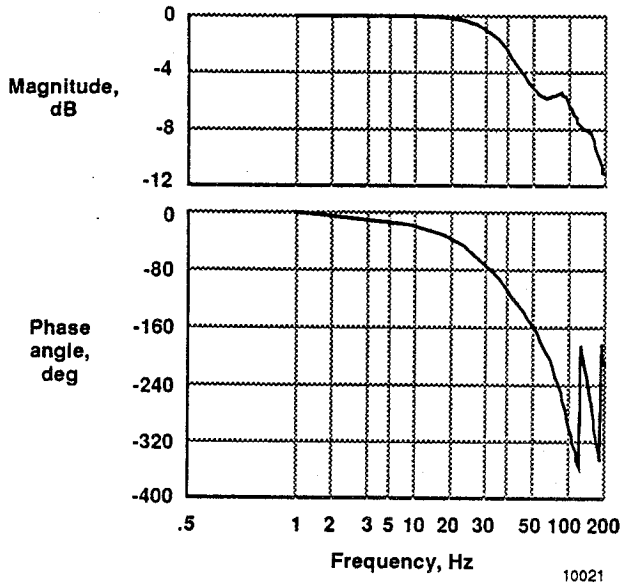

Fig. 3 Analytical predictions of the frequency response.

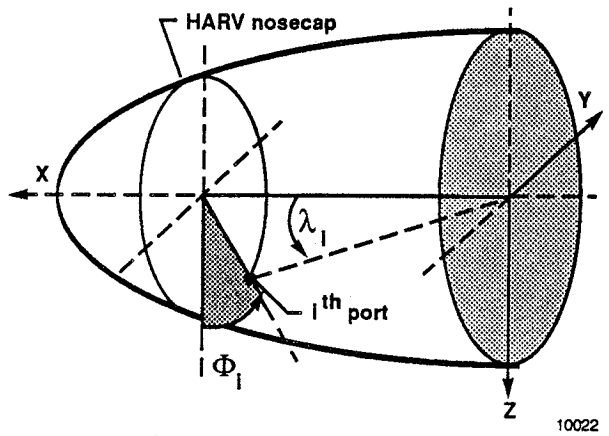

Fig. 4 Coordinate definitions of the ith HI-FADS pressure port.

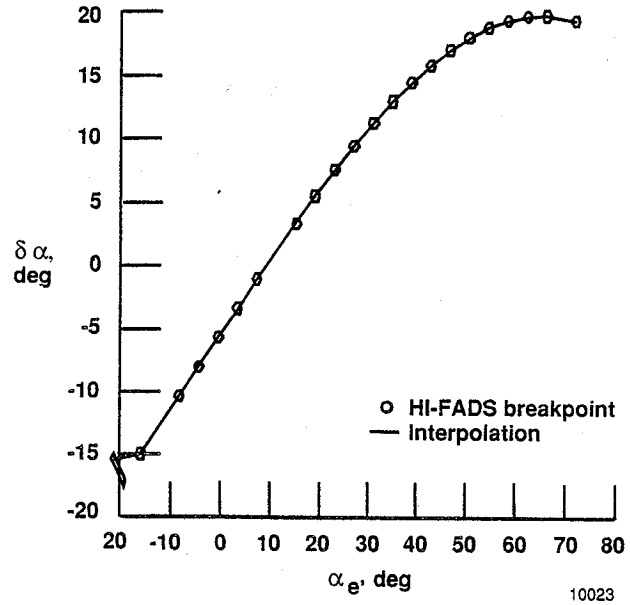

Fig. 5 Calibration results for effective angle-of-attack parameter.

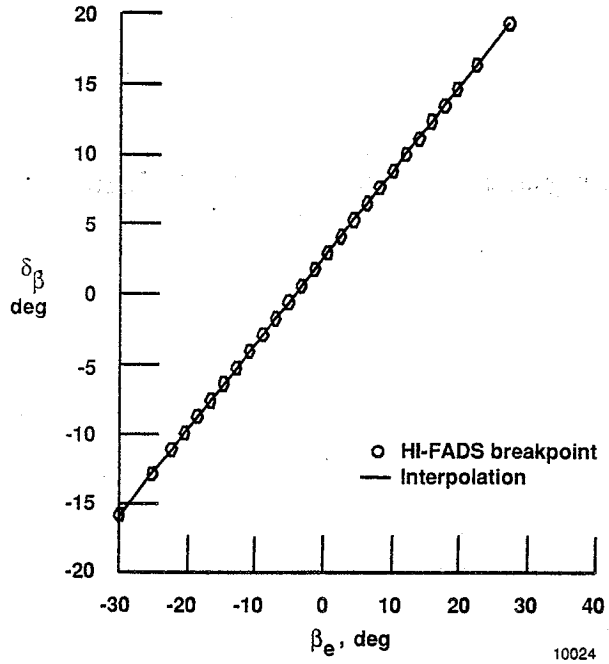

Fig. 6 Calibration results for effective angle-of-sideslip parameter.

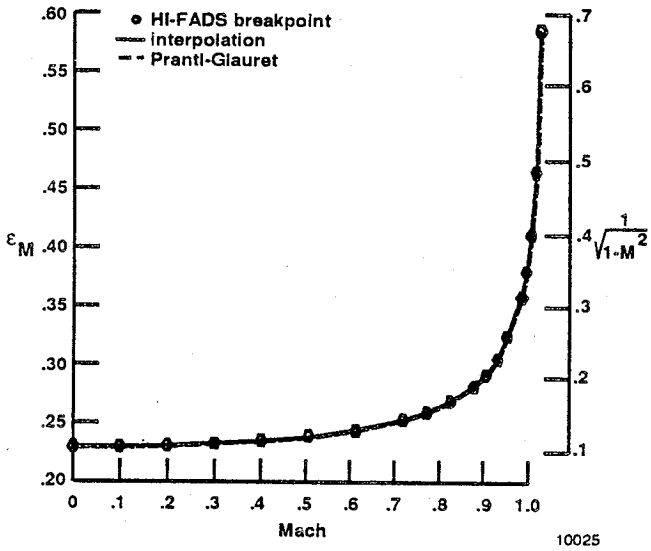

Fig. 7 Calibration results for ϵ_M parameter.

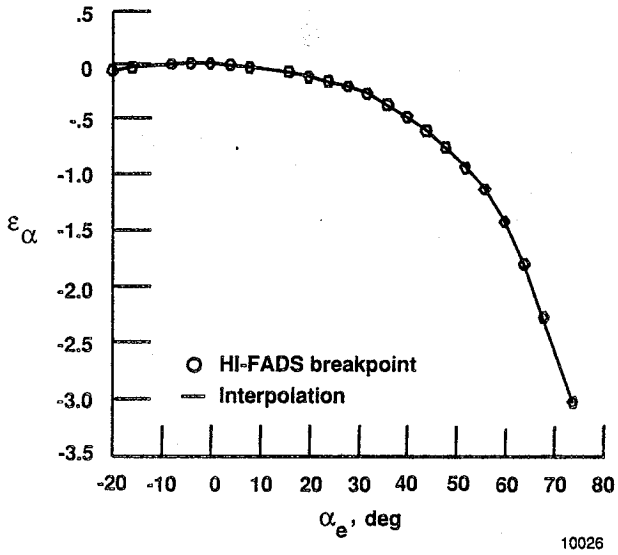

Fig. 8 Calibration results for ϵ_α parameter.

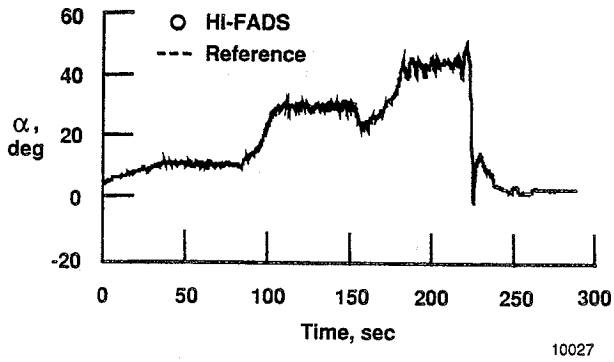

(a) Comparison of HI-FADS and reference angle of attack.

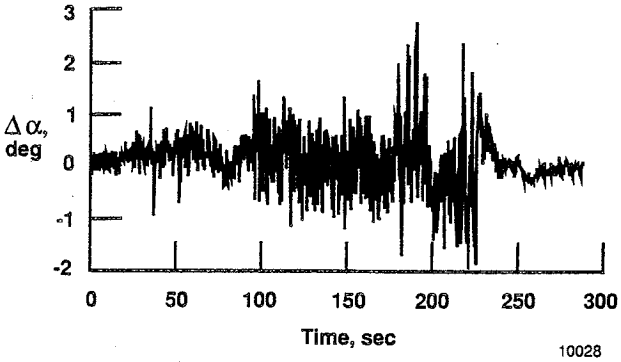

(b) Residual difference between HI-FADS and reference.

Fig. 9 Dutch roll maneuver time history of angle of attack.

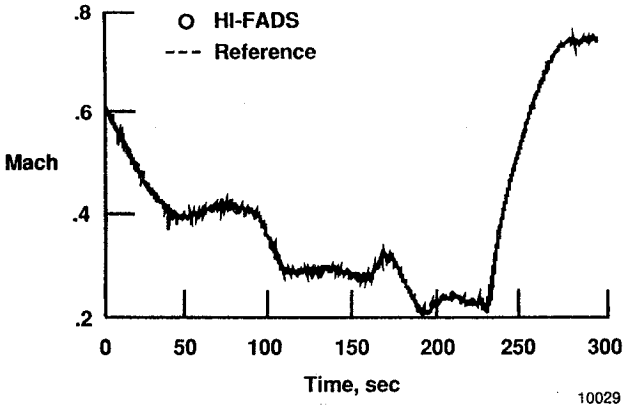

(a) Comparison of HI-FADS and reference Mach number.

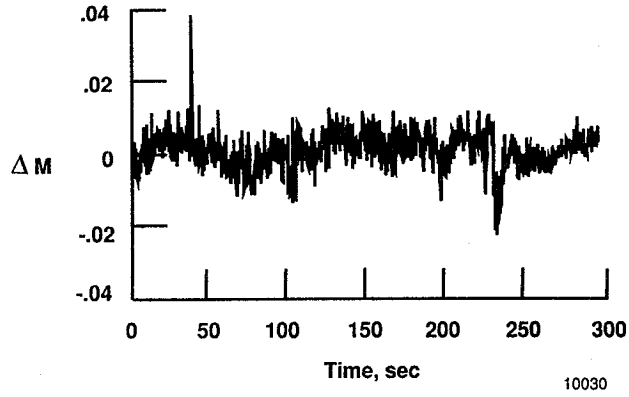

(b) Residual difference between HI-FADS and reference.

Fig. 10 Dutch roll maneuver time history of Mach number.

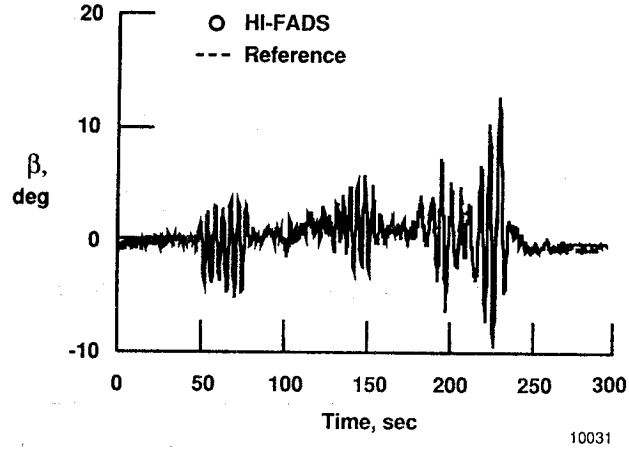

(a) Comparison of HI-FADS and reference angle of sideslip.

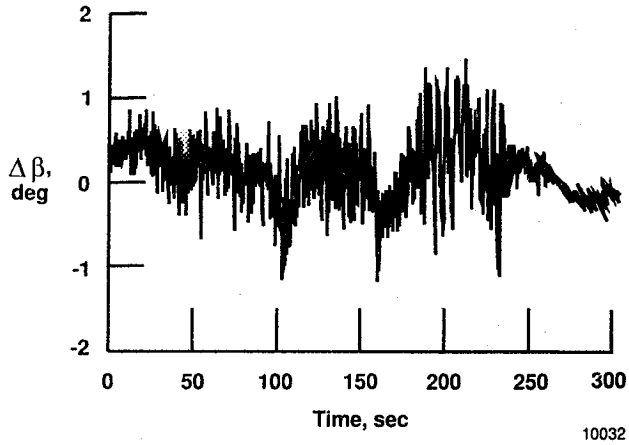

(b) Residual difference between HI-FADS and reference.

Fig. 11 Dutch roll maneuver time history of angle of sideslip.

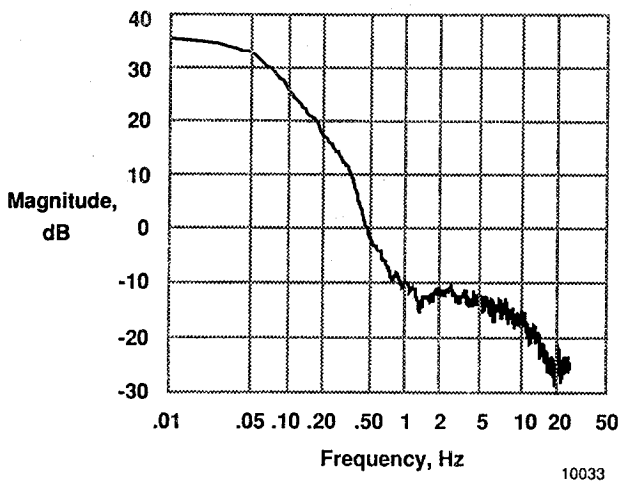

Fig. 12 The HI-FADS data PSD for angle of attack.

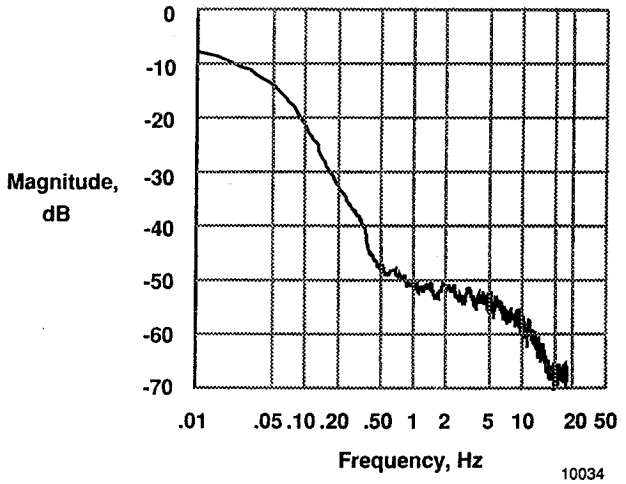

Fig. 13 The HI-FADS data PSD for Mach number.

NASA
National Aeronautics and Space Administration

Report Documentation Page

1. Report No.	2. Government Accession No.	3. Recipient's Catalog No.
NASA TM-101713		

4. Title and Subtitle
Preliminary Results From a Subsonic High Angle-of-Attack Flush Airdata Sensing (HI-FADS) System: Design, Calibration, and Flight Test Evaluation

5. Report Date
January 1990

6. Performing Organization Code

7. Author(s)
Stephen A. Whitmore, Timothy R. Moes, and Terry J. Larson

8. Performing Organization Report No.
H-1583

10. Work Unit No.
RTOP 505-68-71

9. Performing Organization Name and Address
NASA Ames Research Center
Dryden Flight Research Facility
P.O. Box 273, Edwards, CA 93523-5000

11. Contract or Grant No.

13. Type of Report and Period Covered
Technical Memorandum

12. Sponsoring Agency Name and Address
National Aeronautics and Space Administration
Washington, DC 20546

14. Sponsoring Agency Code

15. Supplementary Notes
Prepared as AIAA 90-0232 for presentation at AIAA 28th Aerospace Sciences Meeting, Reno, Nevada, January 8–11, 1990.

16. Abstract

A nonintrusive high angle-of-attack flush airdata sensing (HI-FADS) system was installed and flight-tested on the F-18 high alpha research flight vehicle at the National Aeronautics and Space Administration Ames Research Center's Dryden Flight Research Facility. The system is a matrix of 25 pressure orifices in concentric circles on the nose of the vehicle. The orifices determine angles of attack and sideslip, Mach number, and pressure altitude. Pressure was transmitted from the orifices to an electronically scanned pressure module by lines of pneumatic tubing. The HI-FADS system was calibrated and demonstrated using dutch roll flight maneuvers covering large Mach, angle-of-attack, and sideslip ranges. Reference airdata for system calibration were generated by a minimum variance estimation technique blending measurements from two wingtip airdata booms with inertial velocities, aircraft angular rates and attitudes, precision radar tracking, and meteorological analyses. The pressure orifice calibration was based on identifying empirical adjustments to modified Newtonian flow on a hemisphere. Calibration results are presented. Flight test results used all 25 orifices or used a subset of 9 orifices. Under moderate maneuvering conditions, the HI-FADS system gave excellent results over the entire subsonic Mach number range up to 55° angle of attack. The internal pneumatic frequency response of the system is accurate to beyond 10 Hz. Aerodynamic lags in the aircraft flow field caused some performance degradation during heavy maneuvering.

17. Key Words (Suggested by Author(s))	18. Distribution Statement
Airdata Flush airdata High angle of attack Nonintrusive airdata	Unclassified — Unlimited Subject category 06

19. Security Classif. (of this report)	20. Security Classif. (of this page)	21. No. of pages	22. Price
Unclassified	Unclassified	14	A02

NASA FORM 1626 OCT 86

*For sale by the National Technical Information Service, Springfield, VA 22161-2171.